Genetic and genomic analysis of *Malassezia* reveals transitions in mating-type locus chromosomal organization and early steps in sexual reproduction

Marco A. Coelho[a,1], Giuseppe Ianiri[b,1], Márcia David-Palma[a], Bart Theelen[c], Rohit Goyal[d], Aswathy Narayanan[d], Kaustuv Sanyal[d], Teun Boekhout[c,e] and Joseph Heitman[a,2]

[a]Department of Molecular Genetics and Microbiology, Duke University Medical Center, Durham, NC 27710, USA

[b]Department of Agricultural, Environmental and Food Sciences, University of Molise, Campobasso 86100, Italy

[c]Westerdijk Fungal Biodiversity Institute, Utrecht 3584 CT, The Netherlands

[d]Molecular Mycology Laboratory, Molecular Biology and Genetics Unit, Jawaharlal Nehru Centre for Advanced Scientific Research, Bengaluru 560064, India

[e]College of Science, King Saud University, Riyadh 11451, Saudi Arabia

[1]Equal contribution

[2]Joseph Heitman

Email: heitm001@duke.edu

Author Contributions: M.A.C., G.I., and J.H. designed research; M.A.C. performed genomic, phylogenetic, and transcriptomic analyses; G.I. designed and performed *M. furfur* genetic modifications and RNA-Seq experiments; M.D-P., B.T., A.N., R.G., and K.S. obtained Illumina and Nanopore sequencing data; T.B., provided strains; M.A.C., G.I., and J.H. analyzed data; M.A.C. wrote the paper with contributions from other authors; and J.H. supervised the study.

Competing Interest Statement: The authors declare no competing interest.

Classification: Biological Sciences, Genetics

Keywords: *Malassezia*, Mating-type chromosomes, chromosomal rearrangements, sexual reproduction

This PDF file includes:

Main Text
Figures 1 to 5

Abstract

Fungi in the basidiomycete genus *Malassezia* are the most prevalent eukaryotic microbes resident on the skin of human and other warm-blooded animals and have been implicated in skin diseases and systemic disorders. Analysis of *Malassezia* genomes revealed that key adaptations to the skin microenvironment have a direct genomic basis, and the identification of mating and meiotic genes suggests a capacity to reproduce sexually, even though no sexual cycle has been as yet observed. In contrast to other bipolar or tetrapolar basidiomycetes that have either two linked mating-type-determining (*MAT*) loci or two *MAT* loci on separate chromosomes, in *Malassezia* species studied thus far the two *MAT* loci are arranged in a pseudobipolar configuration (linked on the same chromosome but capable of recombining). By incorporating newly-generated chromosome-level genome assemblies, and an improved *Malassezia* phylogeny, we infer that the pseudobipolar arrangement was the ancestral state of this group and revealed six independent transitions to tetrapolarity, seemingly driven by centromere fission or translocations in centromere-flanking regions. Additionally, in an approach to uncover a sexual cycle, *Malassezia furfur* strains were engineered to express different *MAT* alleles in the same cell. The resulting strains produce hyphae reminiscent of early steps in sexual development and display upregulation of genes associated with sexual development as well as others encoding lipases and a protease potentially relevant for pathogenesis of the fungus. Our study reveals a previously unseen genomic relocation of mating-type loci in fungi and provides insight towards the discovery of a sexual cycle in *Malassezia*, with possible implications for pathogenicity.

Significance Statement

Malassezia, the dominant fungal group of the mammalian skin microbiome, is associated with numerous skin disorders. Sexual development and yeast-to-hyphae transitions, governed by genes at two mating-type (*MAT*) loci, are thought to be important for fungal pathogenicity. However, *Malassezia* sexual reproduction has never been observed. Here, we employed chromosome-level assemblies and comparative genomics to uncover unforeseen transitions in *MAT* loci organization within *Malassezia*, possibly related with fragility of centromeric-associated regions. Additionally, by expressing different *MAT* alleles in the same cell, we show that *Malassezia* can undergo hyphal development and this phenotype is associated with increased expression of key mating genes along with other genes known to be virulence factors, providing a possible connection between hyphal development, sexual reproduction, and pathogenicity.

Introduction

The skin microbiome of humans and other animals is composed of a range of organisms, including viruses, bacteria, and fungi. These organisms interact with host skin cells in different ways, including aiding in defense and immunity, inhibiting the growth of opportunistic or pathogenic organisms, and promoting tissue repair and barrier protection (1). Yeasts of the basidiomycete genus *Malassezia* are the dominant fungal residents of the skin of warm-blooded vertebrates and are usually enriched in sebaceous sites (2, 3). This adaptation is linked to their lipid-dependent growth, which is associated with the loss of key genes for fatty acid synthesis (4, 5). At present, the genus *Malassezia* includes 18 species, with *M. restricta*, *M. arunalokei*, *M. globosa*, *M. sympodialis*, and *M. furfur* more commonly observed on human skin regardless of health or disease status (6). While these species are often considered commensals, they can also be mutualistic or pathogenic. Indeed, *Malassezia* has been linked to various skin disorders (3), and recently implicated in Crohn's disease (7) and progression of colorectal (8) and pancreatic cancer (9). *Malassezia* may also restrict other fungal pathogens, such as *Candida auris*, from colonizing the skin (10). Direct sequencing approaches of diverse environmental sources, such as soil, corals, sponges, deep-sea vents (3, 11), and the skin of healthy human volunteers (12), also revealed that *Malassezia* is more diverse than previously thought.

Whole-genome sequencing of *Malassezia* has provided a wealth of data to explore how this fungal genus has evolved and adapted to the skin microenvironment. Unique genomic features include: (i) small and compact genomes (~7 to 9 Mb) (4, 5); (ii) an increased number of genes encoding lipases, phospholipases, and sphingomyelinases that allow the fungus to exploit abundant extracellular lipids (4, 5); (iii) a low density of repeats and transposable elements possibly associated with loss of the RNA interference machinery (4, 5); (iv) the presence of a dsRNA mycovirus (13, 14); (v) the acquisition of genes via horizontal gene transfer from bacterial lineages commonly found as members of mammalian microbiomes (5, 15); and (vi) karyotypic diversity associated with short centromeres composed of AT-rich sequences (16). These studies also suggested that *Malassezia* species harbor genes necessary to reproduce sexually (5, 17, 18). Despite this, a sexual cycle has yet to be observed in laboratory or natural settings. Sexual

97 reproduction allows natural selection to generate beneficial combinations of alleles and is thus
98 hypothesized to have a role in fungal pathogenesis (19, 20). In addition, sexual development in
99 basidiomycetous yeast lineages is typically marked by a transition from yeast to hyphae, initiated
100 when cells of compatible mating type fuse. This change in morphology has been linked to virulence
101 in several fungal species (21), and has been well studied in smut fungi that affect cereals and other
102 crops (22).

103 Mating-type compatibility in heterothallic basidiomycetes is regulated by two mating-type
104 (*MAT*) loci: the pheromone/receptor (*P/R*) locus, which encodes at least one mating pheromone
105 precursor (Mfa) and one pheromone receptor (Pra) involved in mate recognition, and the
106 homeodomain (*HD*) locus that contains two divergently transcribed homeodomain genes, *HD1*/*bE*
107 and *HD2*/*bW*, which control sexual development following cell fusion (23). To mate and successfully
108 produce offspring, cells must carry different, compatible alleles of both *MAT* loci. In most
109 basidiomycetes, the *P/R* and *HD* loci are located on different chromosomes (tetrapolar
110 configuration), but in some species they have become linked, resulting in an expanded
111 chromosomal region that is highly rearranged and suppressed for recombination between opposite
112 mating types (the bipolar configuration) [reviewed in (23, 24)]. Interestingly, the bipolar
113 configuration is found in several basidiomycetes that are associated with animals or plants, either
114 as pathogens or as commensals (e.g., *Cryptococcus* pathogenic species, the barley smut *Ustilago*
115 *hordei*, and most anther-smut *Microbotryum* species), and it is presumed to have evolved to
116 increase inbreeding (50% chance of compatibility in bipolar compared to 25% in tetrapolar) (23). In
117 contrast, earlier studies of *Malassezia* showed that while the *P/R* and *HD* loci are located on the
118 same chromosome, they are separated by an extended intervening chromosomal region (>100 kb)
119 allowing recombination to still occur to generate novel mating type configurations – an organization
120 known as pseudobipolar (4, 5, 17, 18, 25). Because extant sexual reproduction has yet to be
121 observed for any *Malassezia* species, evidence of recombination is based solely on population
122 genetics studies of natural isolates (17). Furthermore, while *Malassezia* genome sequencing efforts
123 provided an initial view of genome content, most of the available genomes are not assembled as
124 complete chromosomes. Thus, it was unclear if co-localization of the *P/R* and *HD* loci on the same

chromosome is shared by all species and ancestral to this group of fungi, or if there are different mating-type loci configurations across species. It was also unknown if the mating-type genes are associated with the yeast-to-hypha transition, which has been sporadically reported for a few *Malassezia* species in association with disease (26).

Here, genome assemblies were generated and refined for more than half of the known *Malassezia* species, including a new species isolated from the skin of healthy bats. We performed a series of comprehensive cross-species comparative analyses and obtained new insights into the evolution of telomeres, karyotype evolution, and transitions in *MAT* loci chromosomal structure in this fungal genus. Additionally, we show that *M. furfur* can undergo hyphal development when different mating-type alleles are expressed in the same cell following *Agrobacterium*-mediated transformation. Several genes associated with sexual development as well as other genes potentially relevant for pathogenesis were upregulated in these hyphae-producing strains. Our results further suggest a capacity for mating and sexual development in this remarkable group of fungi, with a possible link to pathogenicity.

Results

Improved genomic resources for the *Malassezia* genus and new insight from telomere-to-telomere assemblies

Of the 18 formally described *Malassezia* species, only six had genomes assembled to completion or near completion (**Fig. 1A**). By combining long- (Oxford nanopore) and short-read (Illumina) sequencing, gapless, telomere-to-telomere, assemblies with high base accuracy were generated for 12 *Malassezia* species, including that of a new species recently isolated from bats (*Malassezia* sp. CBS17886) (27), which will be formally described elsewhere (**Fig. 1A**). Based on all assemblies, and excluding the genomes of previously identified hybrid strains (28), the *Malassezia* nuclear genomes range from 7.33 Mb (for *M. restricta*) to 9.31 Mb in size (for *Malassezia* sp. CBS17886) and are organized into 6 to 9 chromosomes (**Fig. 1B** and ***SI Appendix*, Table S1**).

To establish the evolutionary relationships within *Malassezia*, gene prediction and annotation were performed, identifying 1,566 single-copy genes shared across the 20 *Malassezia* species and an outgroup (*Ustilago maydis*). This dataset comprises representatives of all described *Malassezia* species, including the new isolate *Malassezia* sp. CBS17886 and two strains within the *M. furfur* species complex possibly representing two closely related sibling species (28). Phylogenetic reconstructions based on concatenation and coalescence approaches generated completely congruent and robustly supported trees **(Fig. 1** and ***SI Appendix*, Fig. S1**). This analysis recovered the three known main clades (A, B and C) (5, 12) and confirmed the new species status of *Malassezia* sp. CBS17886 given its placement in a distinct branch (clade D). Clades A and B are sister clades, and clade C is the earliest diverging lineage. Furthermore, an interesting relationship was uncovered between *M. furfur* and *Malassezia brasiliensis*, with *M. furfur* parental lineage 1 (P1) and *M. brasiliensis* being more closely related than the two *M. furfur* parental lineages P1 and P2. This builds upon recent findings proposing that the *M. furfur* complex probably

encompasses more than one species and has evolved through a convoluted process involving multiple hybridization events (28).

All *Malassezia* genome assemblies (except *M. dermatis* which was not re-sequenced in this study) had telomeric repeats at the ends of each chromosome. This prompted a closer examination of the telomeric regions, resulting in the recovery of four versions of the telomere-repeat motifs (***SI Appendix*, Table S1**). Apart from *Malassezia pachydermatis* and *Malassezia vespertilionis*, these variants tended to be clade-specific (***SI Appendix*, Table S1**). Upon further examination, distinct species- or clade-specific patterns were observed at the telomere regions. First, in *Malassezia yamatoensis*, 7 of the 16 chromosome ends consist of blocks of telomeric repeats interspersed with unknown repeat sequences (~650 bp). These blocks can span several kilobases (e.g., ~42 kb at the 5' end of chr. 6, ***SI Appendix*, Fig. S2A**) and feature two distinct repeat patterns: a canonical one with multiple tandem copies of the “GGATTA” telomeric repeat motif (3’ end), and a variant form where the motif “GGATGTC” is intermingled with the telomeric repeat motif (TR, type 1 and 2, respectively, ***SI Appendix*, Fig. S2A**). This unusual telomere structure is not seen in the sister species *Malassezia psittaci* and thus suggests a recent change in *M. yamatoensis* telomere structure. Second, in *Malassezia slooffiae* and in species of sub-clades B2 and B3, inverted repeats are found next to the telomeric repeat tract almost invariably present in all chromosomes (**Fig. 1B**, ***SI Appendix*, Fig. S2B** and **Table S1**). Translation of these sequences revealed a large open reading frame in all species except *M. nana*, each predicted to encode a 1,479- to 1,648-amino-acid protein with a reverse transcriptase domain (PF00078). BLASTP searches of these proteins in GenBank produced top matches to hypothetical proteins of other basidiomycetes, including the *Cryptococcus neoformans* Cnl1 element, a non-long-terminal repeat (non-LTR) retrotransposon found predominantly associated with telomeric repeat sequences (29, 30). In *M. slooffiae*, interstitial telomeric repeats are found between copies of the non-LTR element, but this arrangement is absent in other species (***SI Appendix***, **Fig. S2B**). We thus hypothesize that these elements in *Malassezia* are non-LTR retrotransposons that may target telomere repeats, similar to those reported in other eukaryotes, including fungi (29, 31, 32).

192 Previous work in *M. sympodialis* and *M. furfur* established that the region with the lowest
193 GC-content on each chromosome coincides with experimentally validated centromeres (16).
194 Accordingly, inspection of the GC content for the new and updated assemblies found a single
195 discrete region with distinctly low GC content on each chromosome, and these regions were
196 assigned as candidate centromeres (***SI Appendix***, **Fig. S3** and **Dataset S1**). This analysis also
197 revealed a broad variation of the GC-content across species, ranging from 49.6% in *M.*
198 *yamatoensis* to 66.7% in *Malassezia* sp. CBS17886, with most species exhibiting a unimodal GC-
199 content distribution (**Fig. 1C**, and ***SI Appendix*, Fig. S3**). However, six species (*M. sympodialis*, *M.*
200 *dermatis*, *M. caprae*, *M. nana*, *M. equina*, and *M. obtusa*) displayed an unusual wide GC-content
201 distribution and a partially bimodal profile, suggesting their genomes contain a greater proportion
202 of AT-rich regions (**Fig. 1C**, and ***SI Appendix*, Fig S3**). The biological significance of this irregular
203 GC-content distribution in these species is currently unclear and will be addressed in future studies.
204 Overall, this comprehensive genomic dataset will provide an essential resource for further exploring
205 variation across *Malassezia* species and strains, which can now be addressed at gene,
206 chromosomal and population levels.

207

208 **Mating-type loci are conserved across species but exhibit distinct chromosomal**
209 **organization**

210 Studies in *M. globosa*, *M. sympodialis*, and *M. yamatoensis* uncovered a pseudobipolar
211 *MAT* locus configuration with *P/R* and *HD* mating-type loci residing on the same chromosome but
212 separated by large syntenic chromosomal regions (4, 5, 17, 18). Using BLAST searches, we now
213 determined the precise *MAT* loci configurations in all *Malassezia* species. Surprisingly, out of the
214 20 species surveyed, 13 have a pseudobipolar configuration, whereas in the remaining seven the
215 *P/R* and *HD* loci are found on different chromosomes (tetrapolar configuration). Notably, both
216 pseudobipolar and tetrapolar configurations were recovered in all of the clades (**Fig. 1D**), which
217 prompted us to delineate the evolutionary trajectory of the *MAT* loci in *Malassezia*.

By performing synteny analyses we first corroborated and expanded previous findings (4, 5, 17, 18, 28) that the pheromone/receptor (*P/R*) locus contains only two divergently oriented genes encoding a pheromone precursor (*MFA*) and a pheromone receptor (*PRA*) and the *HD* locus comprises two divergently transcribed homeodomain genes designated as *bE* (HD1-type) and *bW* (HD2-type), as found in many basidiomycetes (**Fig. 2A**, and ***SI Appendix*, Fig. S4**) (23). Sequence alignment and phylogenetic analysis determined that the *P/R* locus is biallelic (*a1* or *a2*) as the products of the mating pheromone (Mfa1/Mfa2) and pheromone receptor genes (Pra1/Pra2) clustered into two groups, representing two alternate alleles (**Figs. 2B** and **2C**). Phylogenetic clustering of alleles by mating type across species, rather than clustering by species, is expected for alleles of genes at the *P/R* locus, as they ceased recombining long ago and have since accumulated substitutions independently (known as trans-specific polymorphism) (33). Further examination of the predicted protein sequences of the mature pheromone found that they were indistinguishable between a few closely related species, namely the Mfa2 of *Malassezia dermatis* vs. *Malassezia nana*, and *M. furfur* (P2) vs. *M. brasiliensis* (**Fig. 2C**). However, it is uncertain whether their respective Mfa1 pheromones are also identical.

Next, synteny comparisons showed that both *MAT* loci are embedded within chromosomal regions that are largely conserved across species, although a few species-specific gene insertions/losses are observed in the neighboring regions, suggestive of gene content remodeling as a byproduct of species-specific genome evolution (***SI Appendix*, Fig. S4**). A notable change in *M. brasiliensis* is that the *P/R* locus contains both alternate pheromone receptor genes (*PRA1* and *PRA2*), but only one pheromone gene (*MFA2*) (**Fig. 2A**). This suggests a scenario (illustrated in ***SI Appendix*, Fig. S5**) in which the *M. brasiliensis P/R* locus originated via intra-*MAT* recombination between opposite mating types. In summary, we conclude that despite the different chromosomal organization of *MAT* loci in *Malassezia* (pseudobipolar vs. tetrapolar), the gene content and structure is well conserved.

243 **Transitions in mating-type loci chromosomal organization in *Malassezia***

244 Examination of the species with a pseudobipolar configuration revealed a large range of
245 distances between the two *MAT* loci, from an average of ~145 kb in species of subclade B2, to
246 ~588 kb in species of clade A, and up to 871 kb in *M. slooffiae* (**Fig. 1D**). Along with the presence
247 of tetrapolar species, this led to the hypothesis that the extant pseudobipolar configurations may
248 have resulted from multiple independent events combining the two *MAT* loci on the same
249 chromosome, as previously reported for tetrapolar-to-bipolar transitions in several basidiomycetes
250 (23). Given the *Malassezia* species phylogeny (**Fig. 1A**), if we assume a tetrapolar ancestor and
251 unidirectional transitions, we postulate five independent shifts from tetrapolar to pseudobipolar
252 would have occurred during evolution (Model A; ***SI Appendix*, Fig. S6A**). Alternatively, the
253 observed distance variation between the two *MAT* loci could imply departing from an ancestral
254 pseudobipolar configuration followed by species- or clade-specific intrachromosomal
255 rearrangements (such as large inversions) relocating the two loci within the chromosome. This
256 latter scenario would imply that the tetrapolar *Malassezia* species are a derived state, in which case
257 six independent transitions from pseudobipolar to tetrapolar would have had to occur to explain the
258 extant distribution (Model B; ***SI Appendix*, Fig. S6B**). Lastly, we also considered the possibility of
259 independent transitions occurring in both directions (Model C; ***SI Appendix*, Fig. S6C**).

260 The degree of gene synteny between extant species can reveal essential information about
261 their evolution since their last common ancestor. To ascertain if one of the *MAT* locus evolutionary
262 scenarios is more likely than the others, synteny blocks were reconstructed between all *Malassezia*
263 genomes with SynChro (34), using *M. sympodialis* as reference (***SI Appendix*, Fig. S7**). We
264 focused on comparisons of chromosomes containing *MAT* loci. This analysis revealed
265 pseudobipolar species of clades B, C, and D share conserved synteny for most of the *MAT*
266 chromosomes (**Fig. 3**). In *M. slooffiae* the greater distance between the two *MAT* loci is explained
267 by two large inversions: one relocating the *HD* locus closer to the end of chr. 2 and the other
268 inverting the relative positions of the centromere and the *P/R* locus (**Fig. 3B**). Hence, the similarities
269 between the *MAT* chromosomes of three independently evolving lineages suggest a pseudobipolar

Malassezia ancestor containing a *MAT* chromosome (henceforth referred as Anc1) structurally comparable to that of *M. sympodialis*.

Rearrangements associated with centromere breakage, or translocations in centromere-flanking regions, drove pseudobipolar to tetrapolar transitions

To investigate how pseudobipolar-tetrapolar shifts occurred, we compared *MAT*-containing chromosomes of the tetrapolar species within clades B, C and D with *M. sympodialis* chromosomes. On the basis of centromere predictions and synteny analysis, we hypothesize the transition in *M. pachydermatis* was triggered by a break at the centromere of the predicted Anc1 (**Fig. 4A**, and ***SI Appendix*, Fig. S8**). One of the acentric chromosome arms was rescued by fusion to an ancestral chr. 7 (Anc7), which is mostly structurally intact in *M. slooffiae*, *Malassezia* sp. CBS17886, all species of clades B2, and in *Malassezia japonica*/*M. obtusa* belonging to clade A. The other arm fused to an ancestral chr. 4 (Anc4) conserved in all species of clade B2, but more rearranged in others (**Fig. 4A** and ***SI Appendix*, Figs. S7** and **S8**). Besides relocating the two *MAT* loci onto different chromosomes, this event is associated with karyotype reduction from a predicted ancestor of clades B2-B3 with 8 chromosomes (16). An additional independent event giving rise to the extant 6-chromosome state in *M. pachydermatis* entailed telomere-telomere fusion of chrs. 6 and 8 conserved in clade B2 to generate chr. 5 of *M. pachydermatis* (**Fig. 3C** and ***SI Appendix*, Fig. S8C**). Interestingly, this event was apparently followed by a large inversion whose breakpoints map to the centromere- and telomere-proximal regions of *M. sympodialis* chr. 6. Supporting this series of events is the presence of two genes near the end of chr. 8 in *M. sympodialis*, which are found internalized in *M. pachydermatis* (***SI Appendix*, Fig. S8D**). Although not as yet definitively established, we posit this inversion may have inactivated *CEN6*, thereby stabilizing a presumably dicentric chromosome initially generated upon fusion.

A second independent transition to tetrapolar occurred in clade B1, specifically in the common ancestor of the sibling species *M. restricta*/*M. arunalokei* (**Fig. 3A**). According to synteny

296 analysis, this transition was initiated by a translocation between the centromere-flanking region of
297 Anc1 and a non-centromeric region of Anc7, resulting in the progenitors of chrs. 4 and 5 of *M.*
298 *restricta*/*M. arunalokei* containing, respectively, the *HD* and the *P/R* locus (**Fig. 4B**). A large
299 pericentric inversion subsequently relocated *CEN5* while chr. 4 underwent further rearrangements
300 (**Fig. 4B** and ***SI Appendix*, Fig. S9**).

301 Lastly, *Malassezia cuniculi* (tetrapolar) and *M. slooffiae* (pseudobipolar) are sister species
302 but have diverged considerably since their last common ancestor. Their karyotypes differ markedly:
303 *M. slooffiae* has nine chromosomes, representing the ancestral state of all *Malassezia* species (16),
304 whereas *M. cuniculi* has only six (**Fig. 1A**). The *M. cuniculi* genome is also more rearranged (***SI***
305 ***Appendix*, Fig. S7**); this is particularly evident when comparing the *MAT*-chromosome of *M.*
306 *sympodialis*, which is dispersed over the six chromosomes in *M. cuniculi* as opposed to only three
307 in *M. slooffiae* (***SI Appendix*, Fig. S10**). Despite several rearrangements, many involving the
308 surrounding centromeric regions of Anc1, the centromere itself remained intact, corresponding to
309 *M. cuniculi CEN6* (***SI Appendix*, Fig. S10B**). Hence, the transition to physically unlinked *MAT* loci
310 in *M. cuniculi* appears to be associated with a complex process of karyotypic reduction.

311

312 **Pseudobipolar structure in clade A is not secondarily derived**

313 While our analyses strongly suggests that the pseudobipolar configuration emerged in the
314 *Malassezia* common ancestor, the presence of several tetrapolar species within clade A raised the
315 possibility that a tetrapolar arrangement could be ancestral to this clade, and the pseudobipolar
316 structure in the sibling species *M. yamatoensis/M. psittaci* and *M. furfur/M. brasiliensis* could have
317 represented a more recent reversal to pseudobipolar (Model C in ***SI Appendix*, Fig. S6**). To
318 investigate this, we first performed synteny analyses to model events leading to tetrapolarity of *M.*
319 *vespertilionis*, which branched first within clade A (***SI Appendix*, Fig. S11**). We found a scenario
320 remarkably similar to that described above for *M. restricta*/*M. arunalokei*, entailing a translocation
321 in a centromere-flanking region. However, the translocation involved a different chromosome (chr.

322 2 of *M. sympodialis*) and the predicted translocation breakpoint localizes in the intergenic segment
323 ~5.7 kb upstream of the Anc1 centromere. The resulting chromosome harboring the *P/R* locus later
324 underwent a pericentric inversion followed by breakage close to the centromere, which then healed
325 by *de novo* telomere addition to generate an acrocentric chromosome (chr. 6 of *M. vespertilionis*;
326 ***SI Appendix*, Fig. S11**). The tetrapolar state in *M. vespertilionis* therefore represents another
327 independent transition from pseudobipolar to tetrapolar.

328 As for the other two tetrapolar species in clade A, *M. obtusa* and *M. japonica*, we first noted
329 that their *P/R*- and *HD*-containing chromosomes share extensive blocks of synteny with the *MAT*-
330 chromosome of pseudobipolar species within the *M. furfur*/*M. yamatoensis* clades (**Fig. 3B** and ***SI***
331 ***Appendix*, Fig. S12A**). Similarly, the *MAT*-chromosomes of *M. furfur* and *M. sympodialis*, have
332 large blocks of conserved synteny, but the Anc1 centromere located between the two *MAT* loci was
333 evicted from the *M. furfur*/*M. yamatoensis MAT*-chromosome (**Fig. 3B** and ***SI Appendix*, Fig.**
334 **S12B**). Based on our analysis, this transition is best explained by an inversion and a translocation
335 on Anc1 occurring after the split from the common ancestor with *M. vespertilionis*, but before the
336 divergence of the other species (***SI Appendix*, Fig. S12C**). This inversion repositioned the *P/R*
337 locus further from the *HD* locus and moved the centromere closer to the end of the chromosome.
338 The centromere was then exchanged via translocation between an ancestor of chr. 3 of *M.*
339 *sympodialis* (Anc3) and the centromere-flanking region of the inversion-derived chromosome. As
340 illustrated in ***SI Appendix*, Fig. S12C**, one of the resulting products comprised most of Anc1
341 (including the two *MAT* loci) and a significant portion of Anc3, and likely represents the ancestral
342 *MAT*-chromosome arrangement that emerged after divergence from the last common ancestor with
343 *M. vespertilionis* (designated as AncA in ***SI Appendix*, Fig. S12C**). The other chromosome product
344 inherited the centromere of Anc1 and is structurally identical to the extant chr. 4 of *M. furfur* (or chr.
345 5 in the *M. yamatoensis* clade) suggesting it was retained in these pseudobipolar species. In *M.*
346 *japonica* and *M. obtusa*, this second product underwent further rearrangements but retained the
347 Anc1 centromere and neighboring regions (***SI Appendix*, Fig. S12D**). Finally, the proposed derived
348 *MAT*-chromosome (AncA) also went through various species-specific rearrangements. One such
349 rearrangement independently occurred in *M. japonica* and *M. obtusa*, and seemingly relocated the

350 *P/R* and *HD* loci onto different chromosomes (tetrapolar transition), whereas in *M. furfur*/*M.*
351 *yamatoensis* the two *MAT* loci were retained on the same chromosome (pseudobipolar) (***SI***
352 ***Appendix*, Fig. S12C**). Overall, this indicates that the pseudobipolar configuration is ancestral in
353 *Malassezia*, and all extant tetrapolar species were independently derived from the pseudobipolar
354 ancestral state.

355

356 **Engineered *Malassezia furfur* strains harboring compatible *MAT* alleles undergo hyphal**
357 **development**

358 Studies have demonstrated that *Malassezia* species harbor the key genetic components
359 necessary for mating and meiosis, yet their sexual cycle remains elusive (5, 17, 18). To reassess
360 whether *Malassezia* is able to undergo sexual reproduction, we first crossed several presumably
361 compatible strains of two different *Malassezia* species, *M. furfur* and *M. sympodialis*, on various
362 culture media. Specifically, fusion assays were initially carried out by mixing *M. furfur* strains
363 CBS14141 *ade2*Δ::*NAT* (*MAT a2b1*) x CBS9369 (*MAT a1b2*) (***SI Appendix*, Table S2**). The co-
364 cultures were resuspended in water and plated onto modified minimal medium (mMM, see ***SI***
365 ***appendix***, **SI Material and Methods** for details) supplemented with nourseothricin to select for
366 adenine prototrophy and NAT resistance, respectively, but no colonies were obtained after
367 prolonged incubation. Similarly, *M. sympodialis* strains ATCC42132 NAT^R (*MAT a1b1*) x
368 ATCC44340 NEO^R (*MAT a2b2*) (***SI Appendix*, Table S2**) were mixed and inoculated onto mMM
369 media supplemented with nourseothricin and neomycin/G418, but also in this case no fusion
370 products or meiotic recombinants were recovered.

371 Next, a larger collection of genetically characterized *M. furfur* strains (28) (***SI Appendix*,**
372 **Table S2** and **Fig. S13A**) were crossed in pairwise combinations and examined by microscopy for
373 the possible presence of sexual structures typical of basidiomycete fungi, such as hyphal formation,
374 clamp connections, teliospores, basidia, and basidiospores. Again, no signs of mating were
375 observed in these cases. To circumvent this, we took a genetic approach and fused the genes of

the *P/R a1* locus derived from strain CBS9369, a *NEO* selectable marker, and the genes of the *HD b4* locus derived from strain CBS7710. This transgene was then introduced via *Agrobacterium tumefaciens*-mediated transformation (35) into the presumably compatible *M. furfur* strain CBS14141 (*MAT a2b1*) (**Fig. 5A**, and ***SI Appendix*, Fig. S13**). One NEO^R transformant confirmed by PCR as having both native and exogenous *MAT a* and *b* alleles (***SI Appendix*, Fig. S13D**) was chosen for further analysis. Remarkably, this *M. furfur* transformant produced hyphae on various agar media (stronger on YPD and YT, and fewer hyphae on MS, FA, PDA, and V8 pH7), whereas no hyphal growth was observed in the wild-type (WT) strain CBS1414 under these conditions (***SI Appendix*, Fig. S14A**). This *M. furfur* transformant (*MAT a1a2b1b4*) was named *A*on *B*on (or "solo"), following the nomenclature used for the *U. maydis* solopathogenic strain SG200 engineered to undergo hyphal development and cause smut disease in maize without a mating partner (36). Moreover, when grown in liquid YPD supplemented with compounds reported to promote hyphal formation in *Malassezia* (37) (hereafter referred as "YPD + supplements"; see ***SI Appendix***, **SI Material and Methods**), the *M. furfur* "solo" transformant displayed robust hyphal growth with branches and clamp-like structures (**Fig. 5A** and ***SI Appendix*, Fig. S14C**). Such clamp-like structures in *U. maydis* are formed during the dikaryotic stage and participate in nuclear migration (38). Although the addition of these supplements positively affected the formation of hyphae and clamp-like cells, these structures were also observed, albeit less frequently, in liquid YPD media without the addition of supplements. Last, we noticed that the addition of lipids (e.g., tween and ox-bile) did not affect the ability of the *M. furfur* "solo" transformant to produce hyphae.

To dissect the contribution of each *MAT* locus (*P/R* and *HD*) to filamentation, we then sought to independently introduce the *MAT a1* and *b4* genes into *M. furfur* CBS14141 WT strain. Transformants carrying the *MAT a1* genes were readily obtained, and PCR analysis confirmed the presence of both the native *MAT a2* locus and the exogenous *MAT a1* (***SI Appendix*, Fig. S13D**). A *MAT a1a2b1* strain carrying two compatible alleles of the *P/R* locus was selected and named *A*on *B*off. Curiously, all transformants generated by introducing the *MAT b4* genes alone were not able to maintain stably G418/neomycin genetic resistance and were not analyzed further. Following PCR confirmation, the *M. furfur* WT and derived *A*on *B*off and "solo" strains were grown on YPD

404 agar + supplements and analyzed by scanning electron microscopy for morphological differences.
405 Interestingly, compared to the *M. furfur* WT that only produced yeast cells, both *A*on *B*off and "solo"
406 strains produced highly ramified hyphae with septa, and the presence of clamp-like structures, both
407 fused and unfused (**Fig. 5A** and ***SI Appendix*, Fig. S14**). No obvious morphological differences
408 were observed between the *A*on *B*off and the "solo" mutant under the conditions tested. Taking
409 together, the hyphal growth in *Malassezia* seems to represent the initial stages of sexual
410 development and our genetic analysis provides evidence for a role of the mating-type genes in
411 controlling this process.

412

413 **Key mating genes are upregulated in *M. furfur A*on *B*off and "solo" strains exhibiting hyphal**
414 **growth**

415 To assess if the hyphal phenotype observed in *M. furfur A*on *B*off and *A*on *B*on
416 transformants is associated with activation of genes known to function during sexual reproduction
417 in other basidiomycetes, the transcriptomic profiles of these strains were compared to the *M. furfur*
418 CBS14141 WT, all grown under conditions that promoted hyphae formation (liquid YPD +
419 supplements). RNA-Seq analysis using a false discovery rate (FDR) lower than 5% and $\log_2$ fold
420 change (FC) of 1.0 or greater identified 43 and 144 differentially expressed genes (DEGs),
421 respectively in the *A*on *B*off and "solo" strains compared to the WT, from 4,601 predicted genes
422 (**Fig. 5B**, ***SI Appendix*, Fig. S15**, and **Dataset S2**). Among the DEGs, three are upregulated
423 exclusively in the *A*on *B*off strain, 90 genes have increased expression levels only in the "solo"
424 strain, and 40 genes are upregulated in both *A*on *B*off and "solo" strains (**Fig. 5C**). Gene ontology
425 enrichment analysis did not detect any significantly enrichment among the DEGs in both the *Aon*
426 *B*off and "solo" strains, but several noteworthy genes were identified as discussed below.

427 In the *A*on *B*off strain, three genes were specifically upregulated: one (GLX27_002835)
428 encodes a *Malassezia*-specific protein with unknown function, and the two others encode the
429 endogenous mating-type pheromone (*MFA2*, GLX27_001038a; $\log_2$ FC = 6.59) and pheromone

430 receptor (*PRA2*, GLX27_001038b; $\log_2$ FC = 2.73), which are otherwise expressed at very low
431 levels in the WT (**Dataset S3**). The transcriptional induction of *MFA2* and *PRA2* in the *A*on *B*off
432 strain suggests that a compatible interaction was established by the products of the pheromone
433 (*MFA1*) and receptor (*PRA1*) genes that had been introduced and are expressed in this strain
434 (**Datasets S3** and **S4**). In contrast, no induction of *MFA2* and *PRA2* was detected in the "solo"
435 strain (i.e., the two genes are expressed at WT levels). Compared to the *A*on *B*off strain, the "solo"
436 strain additionally expresses the *bW4* and *bE4* genes (*b4* allele) introduced by transformation, and
437 the native *bW1* and *bE1* genes (*b1* allele) are both upregulated in this context (**Fig. 5B** and **Dataset**
438 **S2**). This presumably allows the formation of an active bW/bE heterodimer, which is likely to
439 negatively affect the transcription levels of the pheromone and receptor genes as found previously
440 in *U. maydis* and *C. neoformans* (39-41).

441 Among the 40 upregulated genes shared by both the *A*on *B*off and "solo" strains, we
442 additionally identified *Malassezia* orthologs of three genes, *CLP1* (GLX27_003783), *KPP6*
443 (GLX27_002769), and *MSB2* (GLX27_000860), which have significant roles during sexual or
444 pathogenic development in the plant pathogen *U. maydis*. *CLP1* (clampless 1) is required for
445 clamp-like cell formation and coordinates the onset of pathogenic development in *U. maydis*
446 through interaction with several other proteins (38). *KPP6* encodes a MAP kinase protein that
447 functions only after cells have fused and developed dikaryotic hyphae and is upregulated by the
448 bE/bW heterodimer. *U. maydis kpp6* mutants develop appressoria (a structure required for plant
449 penetration) but cannot invade the host plant (42). Similarly, the product of *MSB2* is a
450 transmembrane mucin that senses plant surface cues and is essential for appressoria formation in
451 *U. maydis*, acting upstream of the MAP kinase signaling pathway (43). Overall, the increased
452 expression of these genes in the *M. furfur A*on *B*off and "solo" strains relative to wild type suggests
453 they may play key roles in the initiation of the sexual cycle and hyphal development in *Malassezia*.

454 In addition, four genes were upregulated in both *A*on *B*off and "solo" strains that may be
455 significant for the physiology and pathogenicity of *Malassezia*. The first set includes three highly
456 upregulated genes that encode secreted lipases (**Fig. 5B** and **Dataset S2**). Two of these genes,

457 *MFLIP2a* and *MFLIP2b*, are adjacent and result from a gene duplication within clade A (***SI***
458 ***Appendix*, Fig. S16**). Their protein products contain a secretory lipase domain that belongs to the
459 LIP family (PF03583). The third gene (*MFMDL5*) encodes a protein with a lipase class 3 domain
460 (PF01764; ***SI Appendix*, Fig. S17**); the corresponding protein in *M. globosa* (Mgmdl5) can utilize
461 mono-, di-, and tri-glyceride substrates (44). Finally, we observed a striking upregulation of
462 *MFSAP2* (GLX27_000215; $\log_2$ FC = 4.77 and 6.92, for *A*on *B*off and "solo", respectively), which
463 encodes a secretory aspartyl protease. This gene is one of five secretory aspartyl protease (SAP)
464 genes previously identified in *M. furfur* (45) and our own survey indicates that there may be up to
465 9 SAP-like genes in this species (***SI Appendix*, Fig. S18**). A recent study revealed that *MFSAP2*
466 expression is essentially undetectable in *M. furfur* CBS14141 WT, whereas *MFSAP1*
467 (GLX27_000216), which lies adjacent to *MFSAP2* in the genome, is the most highly expressed
468 SAP gene (46). Our data confirmed that *MFSAP1* is highly expressed but not differentially
469 expressed in both mutant and WT strains (GLX27_000216; **Datasets S2** and S3). *M. furfur*
470 *MFSAP1* seems to play an essential role in fungal skin colonization and tissue inflammation, and
471 a compensatory expression of the other SAP genes was not observed when *MFSAP1* was deleted
472 (46). Therefore, the increased expression of *MFSAP2* and three lipase genes in the *A*on *B*off and
473 "solo" strains could represent a life cycle stage-specific response possibly associated with hyphal
474 growth during sexual development.

475

476 **Discussion**

477 Despite a surge in knowledge about *Malassezia* over the last two decades, the natural
478 history, biology, and epidemiology related to colonization and infection by this group of fungi
479 remains largely unexplored. Among the many unknowns about *Malassezia* spp., a prominent one
480 is that a sexual cycle remains to be discovered despite mounting genomic evidence indicating the
481 capacity to undergo mating and meiosis. Our analyses revealed six independent instances of
482 derived tetrapolarity, wherein the *P/R* and *HD* mating-type loci were secondarily relocated onto
483 separate chromosomes from an ancestrally inferred pseudobipolar configuration. Furthermore, by
484 introducing compatible *P/R* and *HD* alleles into *M. furfur*, we engineered a strain capable of initiating

485 a developmental hallmark of basidiomycete sexual reproduction, thereby providing evidence for
486 the presence of an extant sexual cycle in this remarkable group of yeasts.

487 Building on prior studies, the phylogenetic relationships within the *Malassezia* genus were
488 more clearly resolved by integrating whole-genome data, and a new *Malassezia* species isolated
489 from bats was uncovered. Leveraging this high-quality genomic dataset, two genomic features were
490 explored: telomeres and mating-type loci chromosomal organization.

491 We found that telomeric sequences in *Malassezia* are composed of tandem arrays of one
492 of four identified telomere-repeat motif variants. Diversity of telomeric repeat sequences among
493 closely related species is not unprecedented in fungi, particularly in ascomycetous yeasts, where
494 sequence and length variability are even more pronounced and accompanied by rapid evolution of
495 cognate telomere-binding proteins (47, 48). Future identification of the telomerase RNA component
496 in *Malassezia* (a long noncoding RNA that serves as a short template for telomere replication by
497 the telomerase reverse transcriptase catalytic component), using screening strategies as recently
498 reported in *U. maydis* (49), should provide additional support for these telomere sequence
499 differences. Besides telomeric variability, some species contain inverted repeats after the telomeric
500 repeat tract predicted to encode full or partial sequences of non-LTR retrotransposons that might
501 insert into telomeres. While the function and activity of these candidate retrotransposons is
502 presently unknown, studies in other fungi and beyond suggest these elements may cause
503 chromosome instability, yet also provide adaptive benefits (29, 32, 50). In *Drosophila* the loss of
504 the telomerase gene is associated with the replacement of telomeric sequences by tandem
505 retrotransposons, which suggests these elements may counteract chromosome shortening in
506 cases of a dysfunctional telomerase (51). These findings reveal plasticity of *Malassezia*
507 chromosome ends, hinting at a contribution of these regions in shaping the *Malassezia* genomes,
508 with potential impact on speciation and adaptation.

509 Sexual reproduction in fungi is hypothesized to play an important role in pathogenesis as
510 it enables alleles to be reshuffled over generations, thus enabling natural selection to assemble
511 well-adapted allele combinations or break apart deleterious ones (19). The ancestor of all

basidiomycetes likely had unlinked *P/R* and *HD* mating-type loci (tetrapolar), each composed of alternate alleles of a single pair of genes controlling pre- and post-mating mating compatibility (23). However, there is evidence from multiple basidiomycete genera (*Ustilago*, *Cryptococcus*, *Trichosporon*, *Microbotryum*) of *P/R-HD MAT* loci linkage (bipolar) formed through chromosomal translocations or fusions of the ancestral *P/R* and *HD* chromosomes (52-58). This derived state is usually associated with the formation of a large nonrecombining region encompassing multiple genes that are co-inherited during meiosis (24). A recent model proposes that these nonrecombining regions can expand in a stepwise manner due to sheltering of recessive alleles by inversions linked to a permanently heterozygous locus (such as *MAT*), and become highly rearranged between mating types (59). This is reinforced in the case of highly selfing/inbreeding mating systems, where mating occurs preferentially among meiotic products from a single diploid individual. However, the extent to which recombination suppression occurs beyond *MAT* is hypothesized to depend on the duration of the haploid phase (as it enhances purging of deleterious recessive mutations) and the rate of outcrossing (59).

Here we demonstrate that the genetic makeup of the *P/R* and *HD* mating-type loci is conserved across *Malassezia* species, analogous to the archetypal basidiomycete *MAT* loci, and consistent with heterothallic mating. Importantly, by reconstructing synteny blocks between all *Malassezia* genomes, along with centromere identification, we inferred that the *Malassezia* common ancestor was most likely composed of two *MAT* loci located some distance apart on the same chromosome (pseudobipolar) with a centromere located between the two regions. It is uncertain how this ancestral arrangement was established, but this likely involved chromosomal rearrangements, such as translocations, as proposed for other tetrapolar-to-bipolar transitions (52-58). However, this ancestral pseudobipolar arrangement, still seen in most *Malassezia* species albeit with a few modifications, deviates from the typical bipolar configuration. Indeed, at least in *M. sympodialis* (17, 18) and *M. furfur*, for which genome sequences of additional isolates are available, synteny is completely conserved along the *MAT* chromosome between opposite mating types. Consistent with these observations, past studies found alternative allelic combinations of the *P/R* and *HD* loci among isolates of the two species, implying that recombination between the two

540 *MAT* loci occurs (17). In this model, we hypothesize that chromosomal rearrangements within the
541 *P/R-HD* intervening region (e.g., fissions or translocations) are not as detrimental as they would be
542 under a typically bipolar configuration with linked *P/R* and *HD* loci. In agreement, we identified six
543 independent transitions from pseudobipolar to tetrapolar, with five cases involving translocations
544 near the centromere of the ancestral *MAT* chromosome, and one case (*M. pachydermatis*)
545 involving centromere breakage followed by fusion of the acentric chromosome arms to other
546 chromosomes. Centromere breakage is a known mechanism of karyotypic change in *Malassezia*
547 (16), and similar survival by fusion of acentric chromosome arms after centromere fission has been
548 observed in *Schizosaccharomyces pombe* (60) as well as in *Cryptococcus deuterogattii* upon
549 centromere deletion (61). Importantly, and in contrast to other basidiomycetes that usually have
550 large regional centromeres (> 15 kb, often repeat rich), *Malassezia* species have short (< 5 kb-
551 long) regional centromeres, and by virtue of their AT-richness, they seem to constitute fragile sites
552 in the genome (16). We therefore posit that centromeres and, possibly their nearby flanking regions,
553 are more prone to undergo breakage and interchromosomal rearrangements and are thus involved
554 in the repeated transitions from pseudobipolar to tetrapolar in *Malassezia*.

555 The repeated transitions to linked *MAT* loci in basidiomycetes are suggestive of strong
556 selection, which may act to increase gamete compatibility in species with a selfing/inbreeding
557 mating system. Indeed, as mating can only occur when alleles differ at both *MAT* loci, gametes are
558 compatible with only 25% of other gametes in species with two *MAT* loci and two alleles each
559 (tetrapolar), while these odds rise to 50% in species with a single *MAT* locus and two alleles
560 (bipolar). In comparison, the pseudobipolar configuration observed in *Malassezia* results in
561 compatibility odds that are likely between those observed for the bipolar and tetrapolar
562 configurations and depend on the frequency of a single cross-over occurring between the two *MAT*
563 loci during meiosis. Thus, the pseudobipolar system does not seem to be under the same types of
564 selection and constraints as observed in other bipolar basidiomycetes with linked *P/R* and *HD* loci,
565 potentially delaying a transition to a strictly bipolar state. The lack of recombination within bipolar
566 *MAT* alleles of some fungal species (e.g., in *C. neoformans*, the barley smut *U. hordei*, and anther-
567 smut *Microbotryum* species) has also facilitated accumulation of transposable elements in these

568 regions due to a reduced efficacy of selection against deleterious insertions. However, *Malassezia*
569 genomes have a very low density of transposable elements (5), which may pose a further hindrance
570 to formation/stabilization of non-recombining regions. Future studies comparing sequence diversity
571 of *MAT* and the flanking regions from multiple *Malassezia* species and strains, will be fundamental
572 to further understand the evolution of these chromosomal regions.

573 The ability to switch between yeast and hyphal growth is well recognized in numerous
574 fungal pathogens of plants and animals including *U. maydis*, *C. neoformans*, and *Candida albicans*
575 and is known to be associated with virulence in some of these species (22, 62, 63). “Shapeshifting”
576 between different morphologies has been suggested to allow human fungal pathogens to find new
577 sources of nutrients, spread into new areas of the host, and evade the immune system (62).
578 Dimorphism in *Malassezia* was first noticed based on observation of both yeasts and short hyphal
579 filaments on lesional skin sites of patients with pityriasis versicolor (64) (frequently described as
580 the “spaghetti” and “meatballs” appearance). Since then, the presence of *Malassezia* hyphal forms
581 has been reported for several species in both laboratory and clinical settings, with a recent report
582 suggesting that they might be a factor contributing to pathogenesis of seborrheic dermatitis (65).
583 This is intriguing because the hyphal cell type also coincides with the sexual development in
584 dimorphic basidiomycete fungi, which is usually initiated upon mating of compatible partners and
585 regulated by the mating-type genes (23). Unfortunately, in none of the aforementioned studies in
586 *Malassezia* was the relationship between the *MAT* gene composition and dimorphism investigated.

587 Our study provides several lines of evidence for extant sexual development in *Malassezia*
588 beyond the identification of mating and meiotic genes and demonstrates an association between
589 yeast-to-hyphae transition and compatibility at the *MAT* loci. First, engineered haploid *M. furfur*
590 strains harboring compatible *MAT* alleles (*A*on *B*off or *A*on *B*on “solo”) grow as hyphae, unlike the
591 haploid WT strain that grows only as a yeast. Second, the branched hyphal filaments produced by
592 these strains display clamp-like structures typical of a basidiomycete sexual stage. Third, mating-
593 type determining genes are upregulated in *A*on *B*off and “solo” strains suggesting compatibility
594 leading to activation of downstream pathways involved in pheromone response and

595 morphogenesis in other fungi. In the “solo” strain we hypothesize bE/bW heterodimerization
596 generates an active transcriptional regulator that activates/represses other genes, directly or
597 indirectly through interaction with other proteins. Finally, upregulation of *CLP1* in both *A*on *B*off and
598 “solo” strains may mediate steps in sexual reproduction as in in *U. maydis* and *C. neoformans* (38,
599 66).

600 Our transcriptomic analysis further suggests that the dimorphic transition observed in *M.*
601 *furfur A*on *B*off and "solo" strains may further contribute to skin colonization and pathogenicity.
602 Supporting this hypothesis, we detected increased expression of three secreted lipases, adding to
603 the arsenal of lipases expressed and secreted by *M. furfur* yeast cells. Lipases secreted by
604 *Malassezia* breakdown sebum-derived lipids found on human skin (e.g., mono-, di-, and
605 triglycerides) into saturated and unsaturated fatty acids. The saturated fatty acids are taken up by
606 *Malassezia* for growth and proliferation, whereas the irritating unsaturated fatty acids accumulate
607 on the outermost layer of the skin (stratum corneum). This accumulation, which we hypothesize
608 could be further enhanced during hyphal growth, may in turn disrupt permeability of the skin barrier
609 and lead to skin disorders (67). Furthermore, we found that both *M. furfur A*on *B*off and "solo"
610 strains have markedly increased expression of *MFSAP2*, which encodes one of nine putative
611 secretory aspartyl proteases. Recent studies demonstrated that *MFSAP1*, which lies adjacent to
612 *MFSAP2*, is the dominant secretory aspartyl protease in *M. furfur* WT and has critical roles in
613 controlling cell adhesion during colonization and inducing inflammation in barrier-compromised skin
614 (46). Therefore, the *Malassezia* hyphal growth detected associated with initiation of sexual
615 development may have important roles in skin colonization and inflammation, especially in patients
616 with impaired skin barriers, and thus affect its pathogenicity and virulence.

617 Collectively, our work reveals fundamental aspects of *Malassezia* biology. The genomic
618 resources now available for *Malassezia* spp. can be leveraged to identify differences between
619 species and strains, and the characterization of the *MAT* loci across species will assist in
620 determining if different mating types co-exist and thrive on the same host individual. The role of
621 specific genes in mating and hyphae formation can now be directly assessed, applying gene

622 deletion methods recently developed for *Malassezia* (35). Analysis of the hyphae-producing strains
623 in a murine model of *Malassezia* colonization (68) will be an essential next step to gain insight into
624 the role of *Malassezia* cell morphology in skin colonization and disease, and investigate if the skin
625 provides an environment specifically conducive to mating and sexual reproduction.

626 **Materials and Methods**

627 Full details are given in ***SI Appendix***. Briefly, selected *Malassezia* strains were cultured in modified
628 Dixon's media or Leeming & Notman modified media at optimum growth temperature. High-
629 molecular weight DNA for Nanopore sequencing was obtained by a customized
630 cetyltrimethylammonium bromide (CTAB) extraction procedure (69). For Nanopore sequencing,
631 barcoded libraries were obtained using unfragmented DNA and pooled together in MinION or
632 PromethION R9.4.1 flow cells and sequenced. Basecalled reads passing filtering were de-
633 multiplexed and assembled with Canu v2.1.1 (70). Accuracy of draft assemblies was improved with
634 Medaka v1.5.0 or Nanopolish v0.11.2, and further polished with Pilon v1.22 (71) using Illumina
635 paired end reads. The draft assemblies were validated by inspecting read coverage profiles with
636 the Integrative Genomics Viewer after realigning the Canu-corrected and Illumina reads. Gene
637 prediction and annotation on repeat-masked assemblies was performed with the funannotate
638 pipeline v1.8.9, guided with well-annotated proteins of *M. sympodialis* and with RNA-seq where
639 available.

640 *Malassezia* genomes were analyzed and compared via several approaches. For species-
641 tree reconstruction, single copy orthologs were identified across *Malassezia* spp. and the outgroup
642 *U. maydis* with OrthoFinder v2.5.4 (72) and aligned with MAFFT v7.310 (73). A maximum likelihood
643 tree was constructed using a concatenation with gene-based partitioning approach in IQ-TREE
644 v2.1.3 (74) with 1,000 ultrafast bootstraps replicates, and a gene-based coalescence tree was
645 obtained with ASTRAL-MP v5.15.2 (75). Chromosome ends were inspected for the presence of
646 telomeric and other repeats that co-occurred over all or most of the contigs. Centromeric regions
647 were predicted by measuring GC-content in sliding windows of 250 bp (step size = 2) and identifying
648 the corresponding GC-minimum in each contig. GC-content variation and distribution were
649 evaluated with OcculterCut (76) with default settings. Conserved synteny blocks were identified
650 between pairwise combinations of genomes with SynChro (34) setting the block stringency delta to
651 three, and linear synteny plots comparing *MAT* loci and *MAT*-containing chromosomes were
652 performed with Easyfig v2.2.3 (77).

Malassezia furfur strains harboring different combinations of *MAT* alleles (*MAT a1a2b1, A*on *B*off or *MAT a1a2b1b4*, *A*on *B*on "solo") were obtained by *A. tumefaciens*-mediated transformation transforming of *M. furfur* CBS14141 WT with plasmids containing transgenes with the *a1* or the *a1* and *b4* alleles fused to a *NEO* marker and assembled within the T-DNA region of plasmid pGI3 through *in vivo* recombination in *Saccharomyces cerevisiae* (35) (plasmids pGI26 and pGI52, respectively). The resulting transformants and WT were analyzed by light and scanning electron microscopy and subjected to RNA-Seq analysis. RNA extraction of *M. furfur* CBS1414 WT, *A*on *B*off, and "solo" transformants was performed with TRIzol as previously described (15) from three independent cultures grown at 30°C for 2 days in YPD + supplements. To compare the transcriptomic profiles of *A*on *B*off and "solo" transformants relative to WT, 50-bases single end Illumina reads were filtered and trimmed with Trim Galore v0.6.7 and mapped with STAR v.2.7.4a to a reference genome combining the *M. furfur* CBS14141 nuclear genome and the *a1-NEO-b4* transgene sequence. Read count matrices were obtained with featureCounts v2.0.1 and differential expression assessed with DESeq2 v1.36.0 (78) using a FDR < 0.05 and log2 FC > ± 1.0.

Acknowledgments

We thank Drs. Minou Nowrousian, Salomé Leibundgut-Landmann, and John F. Rawls, for critical reading the manuscript and insightful suggestions. We thank Anna Floyd Averette for technical support, and Dr. Fred Dietrich for access to computational resources and dedication. We also wish to thank Dr. Thomas L. Dawson for generating Illumina data for *M. psittaci* and *M. brasiliensis* and Dr. Jeffery M. Lorch for providing isolate CBS17886. This study was supported by NIH/NIAID R01 Grants AI39115 and AI50113, and R21 Grant AI168672, awarded to J.H. *Malassezia* work in the G.I. lab is supported grant LF-OC-22-001060 from the LEO foundation. J.H. is Codirector and Fellow of the CIFAR program Fungal Kingdom: Threats & Opportunities.

References

1. L. Flowers, E. A. Grice, The skin microbiota: balancing risk and reward. *Cell Host Microbe* **28**, 190-200 (2020).
2. K. Findley *et al.*, Topographic diversity of fungal and bacterial communities in human skin. *Nature* **498**, 367-370 (2013).
3. B. Theelen *et al.*, *Malassezia* ecology, pathophysiology, and treatment. *Med. Mycol.* **56**, S10-S25 (2018).
4. J. Xu *et al.*, Dandruff-associated *Malassezia* genomes reveal convergent and divergent virulence traits shared with plant and human fungal pathogens. *Proc. Natl. Acad. Sci. U. S. A.* **104**, 18730-18735 (2007).
5. G. Wu *et al.*, Genus-wide comparative genomics of *Malassezia* delineates its phylogeny, physiology, and niche adaptation on human skin. *PLoS Genet.* **11**, e1005614 (2015).
6. G. Ianiri, S. LeibundGut-Landmann, T. L. Dawson, Jr., *Malassezia*: a commensal, pathogen, and mutualist of human and animal skin. *Annu. Rev. Microbiol.* **76**, 757-782 (2022).
7. J. J. Limon *et al.*, *Malassezia* Is associated with Crohn's disease and exacerbates colitis in mouse models. *Cell Host Microbe* **25**, 377-388 e376 (2019).
8. R. Gao *et al.*, Dysbiosis signature of mycobiota in colon polyp and colorectal cancer. *Eur. J. Clin. Microbiol. Infect. Dis.* **36**, 2457-2468 (2017).
9. B. Aykut *et al.*, The fungal mycobiome promotes pancreatic oncogenesis via activation of MBL. *Nature* **574**, 264-267 (2019).
10. D. M. Proctor *et al.*, Integrated genomic, epidemiologic investigation of *Candida auris* skin colonization in a skilled nursing facility. *Nat. Med.* **27**, 1401-1409 (2021).
11. A. Amend, From dandruff to deep-sea vents: *Malassezia*-like fungi are ecologically hyper-diverse. *PLoS Pathog.* **10**, e1004277 (2014).
12. S. Saheb Kashaf *et al.*, Integrating cultivation and metagenomics for a multi-kingdom view of skin microbiome diversity and functions. *Nat. Microbiol.* **7**, 169-179 (2022).
13. S. Applen Clancey, F. Ruchti, S. LeibundGut-Landmann, J. Heitman, G. Ianiri, A novel mycovirus evokes transcriptional rewiring in the fungus *Malassezia* and stimulates beta interferon production in macrophages. *mBio* **11** (2020).
14. M. Park *et al.*, A novel virus alters gene expression and vacuolar morphology in *Malassezia* cells and induces a TLR3-mediated inflammatory immune response. *mBio* **11** (2020).
15. G. Ianiri *et al.*, HGT in the human and skin commensal *Malassezia*: A bacterially derived flavohemoglobin is required for NO resistance and host interaction. *Proc. Natl. Acad. Sci. U. S. A.* **117**, 15884-15894 (2020).
16. S. R. Sankaranarayanan *et al.*, Loss of centromere function drives karyotype evolution in closely related *Malassezia* species. *Elife* **9** (2020).
17. A. Gioti *et al.*, Genomic insights into the atopic eczema-associated skin commensal yeast *Malassezia sympodialis*. *mBio* **4**, e00572-00512 (2013).
18. Y. Zhu *et al.*, Proteogenomics produces comprehensive and highly accurate protein-coding gene annotation in a complete genome assembly of *Malassezia sympodialis*. *Nucleic Acids Res.* **45**, 2629-2643 (2017).
19. K. Nielsen, J. Heitman, Sex and virulence of human pathogenic fungi. *Adv. Genet.* **57**, 143-173 (2007).
20. J. Heitman, D. A. Carter, P. S. Dyer, D. R. Soll, Sexual reproduction of human fungal pathogens. *Cold Spring Harb. Perspect. Med.* **4** (2014).
21. C. A. Morrow, J. A. Fraser, Sexual reproduction and dimorphism in the pathogenic basidiomycetes. *FEMS Yeast Res.* **9**, 161-177 (2009).
22. T. Brefort *et al.*, *Ustilago maydis* as a Pathogen. *Annu. Rev. Phytopathol.* **47**, 423-445 (2009).
23. M. A. Coelho, G. Bakkeren, S. Sun, M. E. Hood, T. Giraud, Fungal Sex: the Basidiomycota. *Microbiol. Spectr.* **5** (2017).
24. F. E. Hartmann *et al.*, Recombination suppression and evolutionary strata around mating-type loci in fungi: documenting patterns and understanding evolutionary and mechanistic causes. *New Phytol.* **229**, 2470-2491 (2021).

25. M. A. Coelho, J. P. Sampaio, P. Gonçalves, Living and thriving on the skin: *Malassezia* genomes tell the story. *mBio* **4**, e00117-00113 (2013).
26. G. Gaitanis, P. Magiatis, M. Hantschke, I. D. Bassukas, A. Velegraki, The *Malassezia* genus in skin and systemic diseases. *Clin. Microbiol. Rev.* **25**, 106-141 (2012).
27. J. M. Lorch *et al.*, *Malassezia vespertilionis* sp. nov.: a new cold-tolerant species of yeast isolated from bats. *Persoonia* **41**, 56-70 (2018).
28. B. Theelen *et al.*, Multiple hybridization events punctuate the evolutionary trajectory of *Malassezia furfur*. *mBio* **13**, e0385321 (2022).
29. S. J. Priest *et al.*, Uncontrolled transposition following RNAi loss causes hypermutation and antifungal drug resistance in clinical isolates of *Cryptococcus neoformans*. *Nat. Microbiol.* **7**, 1239-1251 (2022).
30. G. Janbon *et al.*, Characterizing the role of RNA silencing components in *Cryptococcus neoformans*. *Fungal Genet. Biol.* **47**, 1070-1080 (2010).
31. H. Fujiwara, M. Osanai, T. Matsumoto, K. K. Kojima, Telomere-specific non-LTR retrotransposons and telomere maintenance in the silkworm, *Bombyx mori*. *Chromosome Res.* **13**, 455-467 (2005).
32. J. H. Starnes, D. W. Thornbury, O. S. Novikova, C. J. Rehmeyer, M. L. Farman, Telomere-targeted retrotransposons in the rice blast fungus *Magnaporthe oryzae*: agents of telomere instability. *Genetics* **191**, 389-406 (2012).
33. B. Devier, G. Aguileta, M. E. Hood, T. Giraud, Ancient trans-specific polymorphism at pheromone receptor genes in basidiomycetes. *Genetics* **181**, 209-223 (2009).
34. G. Drillon, A. Carbone, G. Fischer, SynChro: a fast and easy tool to reconstruct and visualize synteny blocks along eukaryotic chromosomes. *PLoS ONE* **9**, e92621 (2014).
35. G. Ianiri, A. F. Averette, J. M. Kingsbury, J. Heitman, A. Idnurm, Gene function analysis in the ubiquitous human commensal and pathogen *Malassezia* genus. *mBio* **7** (2016).
36. J. Kämper *et al.*, Insights from the genome of the biotrophic fungal plant pathogen *Ustilago maydis*. *Nature* **444**, 97-101 (2006).
37. M. R. Saadatzadeh, H. R. Ashbee, K. T. Holland, E. Ingham, Production of the mycelial phase of *Malassezia* in vitro. *Med. Mycol.* **39**, 487-493 (2001).
38. M. Scherer, K. Heimel, V. Starke, J. Kämper, The Clp1 protein is required for clamp formation and pathogenic development of *Ustilago maydis*. *Plant Cell* **18**, 2388-2401 (2006).
39. C. M. Hull, M. J. Boily, J. Heitman, Sex-specific homeodomain proteins Sxi1α and Sxi2a coordinately regulate sexual development in *Cryptococcus neoformans*. *Eukaryot. Cell* **4**, 526-535 (2005).
40. C. Laity, L. Giasson, R. Campbell, J. Kronstad, Heterozygosity at the *b* mating-type locus attenuates fusion in *Ustilago maydis*. *Curr. Genet.* **27**, 451-459 (1995).
41. M. Urban, R. Kahmann, M. Bölker, Identification of the pheromone response element in *Ustilago maydis*. *Mol. Gen. Genet.* **251**, 31-37 (1996).
42. A. Brachmann, J. Schirawski, P. Muller, R. Kahmann, An unusual MAP kinase is required for efficient penetration of the plant surface by *Ustilago maydis*. *EMBO J.* **22**, 2199-2210 (2003).
43. D. Lanver, A. Mendoza-Mendoza, A. Brachmann, R. Kahmann, Sho1 and Msb2-related proteins regulate appressorium development in the smut fungus *Ustilago maydis*. *Plant Cell* **22**, 2085-2101 (2010).
44. B. Sommer, D. P. Overy, B. Haltli, R. G. Kerr, Secreted lipases from *Malassezia globosa*: recombinant expression and determination of their substrate specificities. *Microbiology* **162**, 1069-1079 (2016).
45. S. E. Poh *et al.*, Identification of *Malassezia furfur* secreted aspartyl protease 1 (MfSAP1) and its role in extracellular matrix degradation. *Front. Cell. Infect. Microbiol.* **10**, 148 (2020).
46. J. P. Z. Goh *et al.*, The human pathobiont *Malassezia furfur* secreted protease Mfsap1 regulates cell dispersal and exacerbates skin inflammation. *Proc. Natl. Acad. Sci. U. S. A.* **119**, e2212533119 (2022).
47. N. F. Lue, Plasticity of telomere maintenance mechanisms in yeast. *Trends Biochem. Sci.* **35**, 8-17 (2010).
48. F. Cervenak *et al.*, Identification of telomerase RNAs in species of the *Yarrowia* clade provides insights into the co-evolution of telomerase, telomeric repeats and telomere-binding proteins. *Sci. Rep.* **9**, 13365 (2019).

49. D. Logeswaran *et al.*, Biogenesis of telomerase RNA from a protein-coding mRNA precursor. *Proc. Natl. Acad. Sci. U. S. A.* **119**, e2204636119 (2022).
50. M. Rahnama *et al.*, Telomere roles in fungal genome evolution and adaptation. *Front. Genet.* **12**, 676751 (2021).
51. H. Biessmann *et al.*, Addition of telomere-associated HeT DNA sequences "heals" broken chromosome ends in *Drosophila*. *Cell* **61**, 663-673 (1990).
52. J. A. Fraser *et al.*, Convergent evolution of chromosomal sex-determining regions in the animal and fungal kingdoms. *PLoS Biol.* **2**, e384 (2004).
53. S. Sun *et al.*, Fungal genome and mating system transitions facilitated by chromosomal translocations involving intercentromeric recombination. *PLoS Biol.* **15**, e2002527 (2017).
54. S. Branco *et al.*, Evolutionary strata on young mating-type chromosomes despite the lack of sexual antagonism. *Proc. Natl. Acad. Sci. U. S. A.* **114**, 7067-7072 (2017).
55. S. Branco *et al.*, Multiple convergent supergene evolution events in mating-type chromosomes. *Nat. Commun.* **9**, 2000 (2018).
56. N. Lee, G. Bakkeren, K. Wong, J. E. Sherwood, J. W. Kronstad, The mating-type and pathogenicity locus of the fungus *Ustilago hordei* spans a 500-kb region. *Proc. Natl. Acad. Sci. U. S. A.* **96**, 15026-15031 (1999).
57. F. Rabe *et al.*, A complete toolset for the study of *Ustilago bromivora* and *Brachypodium* sp. as a fungal-temperate grass pathosystem. *Elife* **5** (2016).
58. S. Sun, M. A. Coelho, J. Heitman, M. Nowrousian, Convergent evolution of linked mating-type loci in basidiomycete fungi. *PLoS Genet.* **15**, e1008365 (2019).
59. P. Jay, E. Tezenas, A. Véber, T. Giraud, Sheltering of deleterious mutations explains the stepwise extension of recombination suppression on sex chromosomes and other supergenes. *PLoS Biol.* **20**, e3001698 (2022).
60. K. Ishii *et al.*, Heterochromatin integrity affects chromosome reorganization after centromere dysfunction. *Science* **321**, 1088-1091 (2008).
61. K. Schotanus, J. Heitman, Centromere deletion in *Cryptococcus deuterogattii* leads to neocentromere formation and chromosome fusions. *Elife* **9** (2020).
62. K. Min, A. M. Neiman, J. B. Konopka, Fungal pathogens: shape-shifting invaders. *Trends Microbiol.* **28**, 922-933 (2020).
63. J. Klose, M. M. de Sá, J. W. Kronstad, Lipid-induced filamentous growth in *Ustilago maydis*. *Mol. Microbiol.* **52**, 823-835 (2004).
64. M. A. Gordon, The lipophilic mycoflora of the skin. I. In vitro culture of *Pityrosporum Orbiculare* n. sp. *Mycologia* **43**, 524-535 (1951).
65. J. Li *et al.*, Presence of *Malassezia* hyphae Is correlated with pathogenesis of seborrheic dermatitis. *Microbiol. Spectr.* **10**, e0116921 (2022).
66. J. L. Ekena, B. C. Stanton, J. A. Schiebe-Owens, C. M. Hull, Sexual development in *Cryptococcus neoformans* requires *CLP1*, a target of the homeodomain transcription factors Sxi1α and Sxi2**a**. *Eukaryot. Cell* **7**, 49-57 (2008).
67. M. Park, S. Park, W. H. Jung, Skin commensal fungus *Malassezia* and its lipases. *J. Microbiol. Biotechnol.* **31**, 637-644 (2021).
68. F. Sparber *et al.*, The skin commensal yeast *Malassezia* triggers a type 17 response that coordinates anti-fungal immunity and exacerbates skin inflammation. *Cell Host Microbe* **25**, 389-403 e386 (2019).
69. V. Yadav, S. Sun, M. A. Coelho, J. Heitman, Centromere scission drives chromosome shuffling and reproductive isolation. *Proc. Natl. Acad. Sci. U. S. A.* **117**, 7917-7928 (2020).
70. S. Koren *et al.*, Canu: scalable and accurate long-read assembly via adaptive k-mer weighting and repeat separation. *Genome Res.* **27**, 722-736 (2017).
71. B. J. Walker *et al.*, Pilon: an integrated tool for comprehensive microbial variant detection and genome assembly improvement. *PLoS ONE* **9**, e112963 (2014).
72. D. M. Emms, S. Kelly, OrthoFinder: phylogenetic orthology inference for comparative genomics. *Genome Biol.* **20**, 238 (2019).
73. K. Katoh, D. M. Standley, MAFFT multiple sequence alignment software version 7: improvements in performance and usability. *Mol. Biol. Evol.* **30**, 772-780 (2013).
74. B. Q. Minh *et al.*, IQ-TREE 2: new models and efficient methods for phylogenetic inference in the genomic era. *Mol. Biol. Evol.* **37**, 1530-1534 (2020).

843 75. J. Yin, C. Zhang, S. Mirarab, ASTRAL-MP: scaling ASTRAL to very large datasets using
844 randomization and parallelization. *Bioinformatics* **35**, 3961-3969 (2019).
845 76. A. C. Testa, R. P. Oliver, J. K. Hane, OcculterCut: a comprehensive survey of AT-rich
846 regions in fungal genomes. *Genome Biol. Evol.* **8**, 2044-2064 (2016).
847 77. M. J. Sullivan, N. K. Petty, S. A. Beatson, Easyfig: a genome comparison visualizer.
848 *Bioinformatics* **27**, 1009-1010 (2011).
849 78. M. I. Love, W. Huber, S. Anders, Moderated estimation of fold change and dispersion for
850 RNA-seq data with DESeq2. *Genome Biol.* **15**, 550 (2014).

Figures

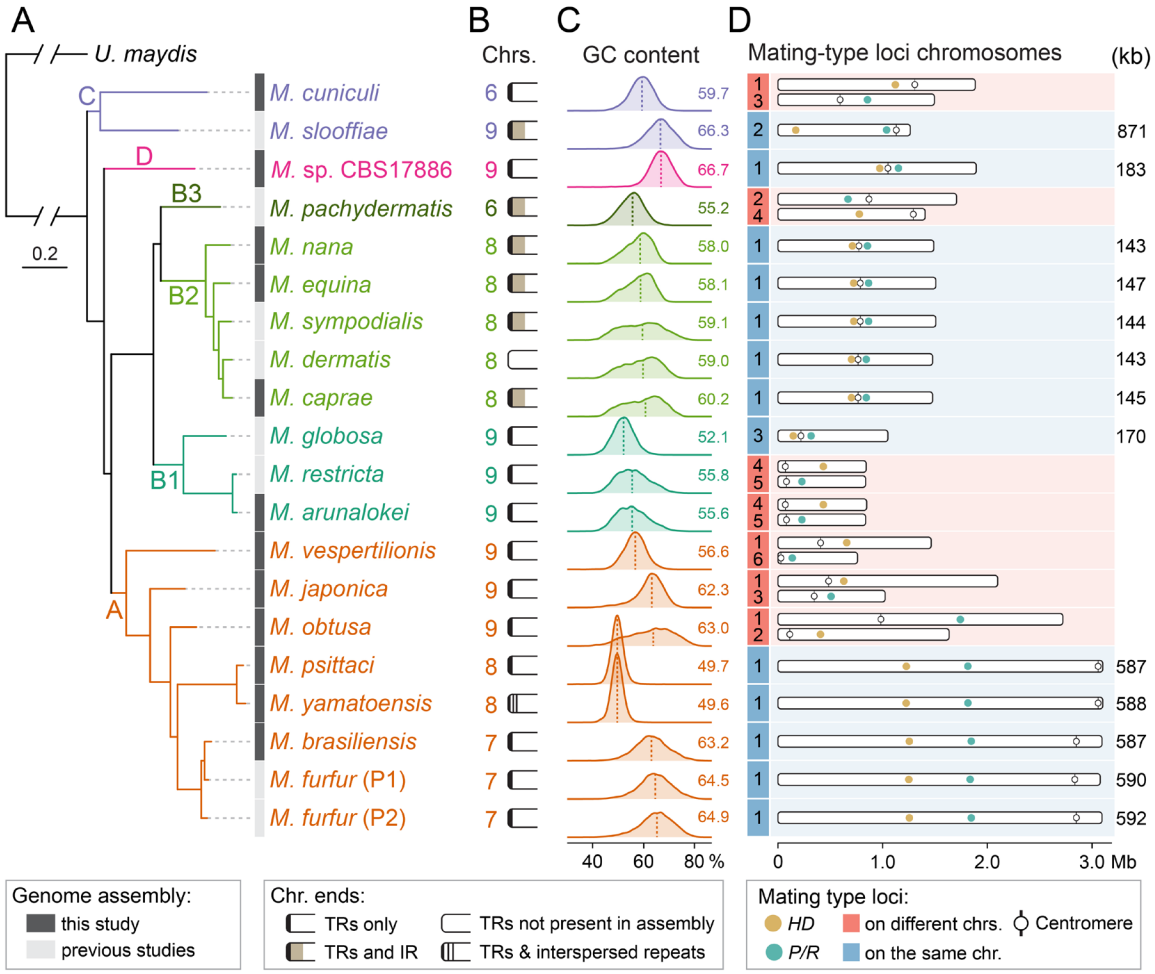

Fig. 1. Phylogenetic diversity, karyotypic variation, and mating-type loci organization in *Malassezia*. (A) Species phylogeny inferred by maximum likelihood analysis using a concatenation-based approach on a data matrix composed of protein alignments of 1,566 single-copy genes shared across all *Malassezia* species and an outgroup (*Ustilago maydis*). All branches are 100% supported (SH-aLRT and UFboot tests; see ***SI Appendix,* Fig. S1**). Branch lengths are given in number of substitutions per site (scale bar). Complete genome sequences obtained in this study are marked in dark grey. (B) Chromosome number and structure of the chromosome ends. All assemblies, with the exception of *M. dermatis*, are assembled telomere-to-telomere. In some species, chromosome ends present inverted repeats (IR) beyond the telomeric-repeat sequences (TRs). In *M. yamatoensis*, some of the chromosome ends are expanded and display TRs motifs interspersed with other repeat sequences (see ***SI Appendix,* Fig. S2**). (C) Frequency distribution of GC content across species. Mean GC values are shown next to the plot and depicted by vertical dashed lines. Some species present constant GC content across the genome (e.g., *M. yamatoensis*), while others (e.g., *M. obtusa*) have an uneven distribution. (D) Chromosomal localization of the two mating-type loci (pheromone/receptor locus – *P/R*, and homeodomain transcription factor locus – *HD*) with distance between the two loci shown in kb on the right.

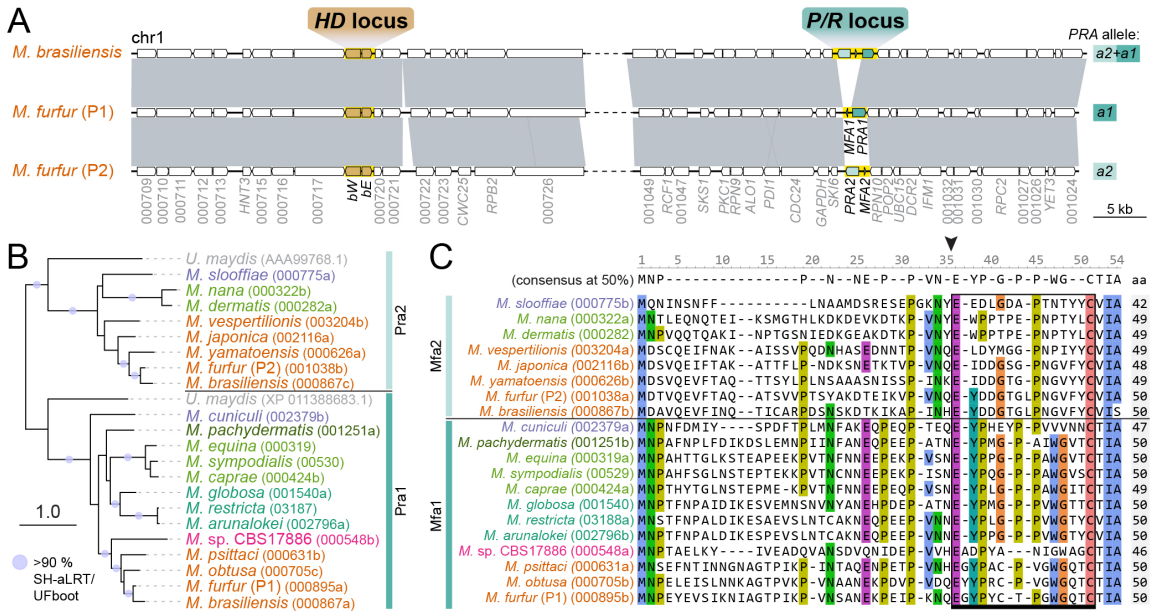

Fig. 2. *MAT* loci structure and mating-type genes in *Malassezia*. (A) Synteny analysis comparing the chromosomal regions encompassing the *HD* and *P/R MAT* loci in two *M. furfur* representatives with different mating types and *M. brasiliensis*. The *P/R* and *HD* loci are highlighted in yellow. With the exception of *M. brasiliensis* that contains two alternate pheromone receptor genes (*PRA1* and *PRA2*) and one pheromone gene (*MFA2*) at the *P/R* locus, the gene structure of the two *MAT* loci is conserved across the genus (see additional comparisons on ***SI Appendix,* Fig. S4**). (B) Maximum likelihood phylogeny of *Malassezia* and *Ustilago maydis* Pra1 and Pra2 pheromone receptors showing clustering into two main groups representing the two alternate alleles. The tree was constructed with IQ-TREE2 (model LG+F+I+R6) and rooted at the midpoint. Internal branch support was assessed by 10,000 replicates of Shimodaira–Hasegawa approximate likelihood ratio test (SH-aLRT) and ultrafast bootstrap (UFboot) and well supported branches (>90%) are depicted by gray circles. Branch lengths are given in number of substitutions per site. (C) Sequence alignment of Mfa1 and Mfa2 pheromone precursors. The black arrowhead denotes the predicted cleavage site, giving rise to the peptide moiety of the mature pheromone (indicated by a black bar).

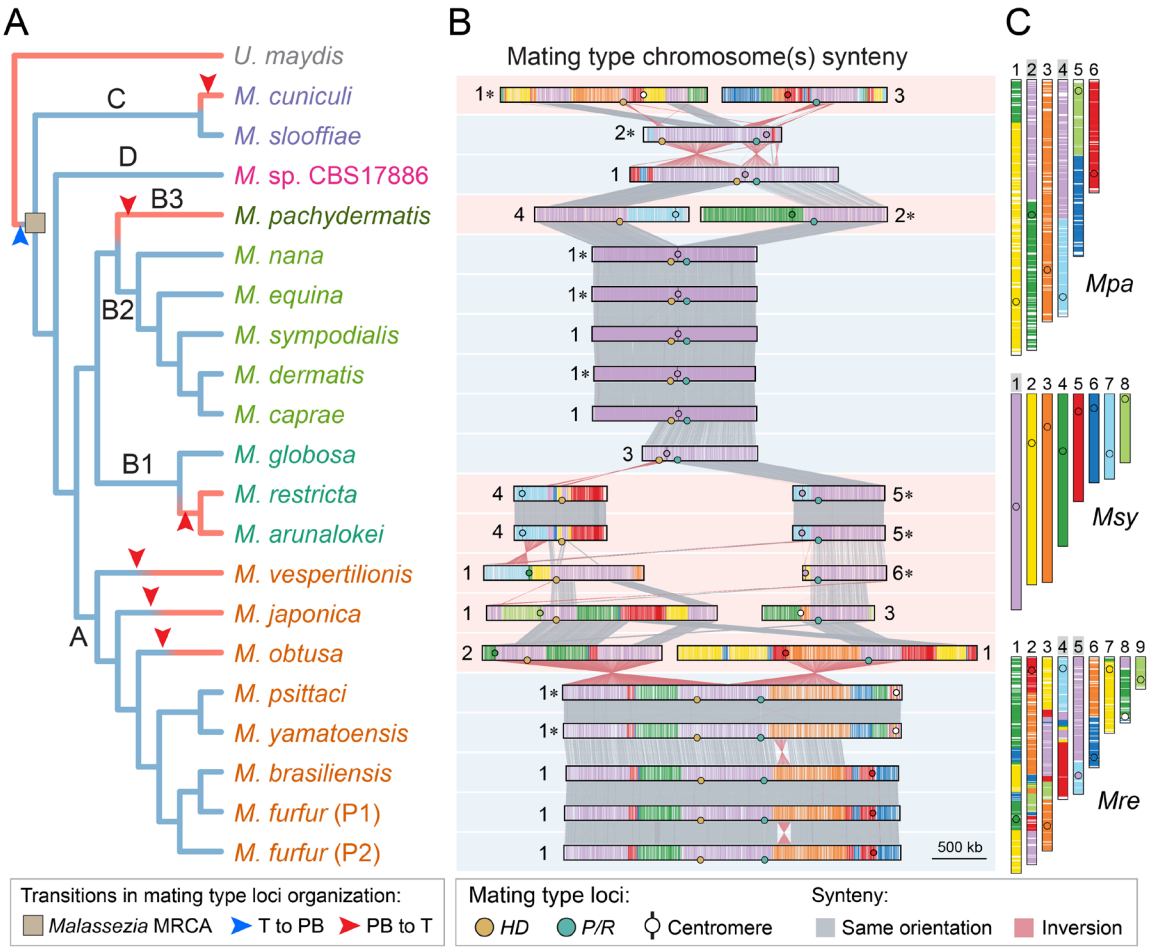

Fig. 3. Proposed transitions in mating-type loci chromosomal organization in *Malassezia*. (A) Species-tree topology depicting hypothesized transition events in mating-type loci organization. A transition from tetrapolar (T) to pseudobipolar (PB) depicted by a blue arrowhead is proposed to have occurred only once in the *Malassezia* most recent common ancestor (MRCA) from which all the tetrapolar species have independently derived (depicted by red arrowheads in the tree branches). (B) Synteny analysis comparing the chromosomes containing the *HD* and *P/R MAT* loci across species. Chromosomes displayed in reversed orientation are marked by asterisks. (C) Chromosome structure differences between *M. sympodialis* (*Msy*; used as reference) and two other *Malassezia* species (*M. restricta* – *Mre*, and *M. pachydermatis* – *Mpa*) are shown as an example (see ***SI Appendix*, Figs. S6 and S7** for additional comparisons and other hypothesized models).

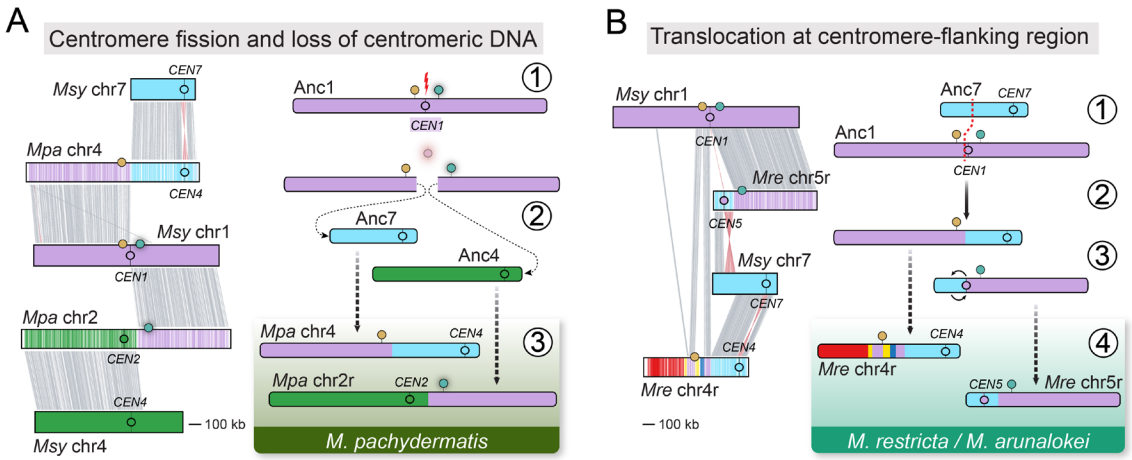

Fig. 4. Main mechanisms underlying the pseudobipolar to tetrapolar transitions. (A) Synteny analysis (left side) between *M. sympodialis* and *M. pachydermatis MAT*-containing chromosomes indicates that the pseudobipolar to tetrapolar transition in *M. pachydermatis* possibly occurred due to centromere breakage on an ancestral chromosome (Anc1) containing the two *MAT* loci regions (*P/R*, green circle; *HD*, golden circle) (step 1). This event resulted in centromere loss, and the resulting chromosome arms were rescued by fusion to other chromosomes (step 2) thereby relocating the *P/R* and *HD* loci onto different chromosomes (step 3). (B) Differently, the transition in the common ancestor of *M. restricta* and *M. arunalokei* is hypothesized to have involved a translocation at the pericentromeric region of the Anc1 with a non-centromeric region of another chromosome (depicted here as the Anc7) (steps 1 and 2). Synteny analysis between *M. sympodialis* and *M. restricta* (left side) further indicate that an additional pericentric inversion occurred in the derived *P/R*-containing chromosome and further rearrangements reshaped the *HD*-containing chromosome during evolution (steps 3 and 4).

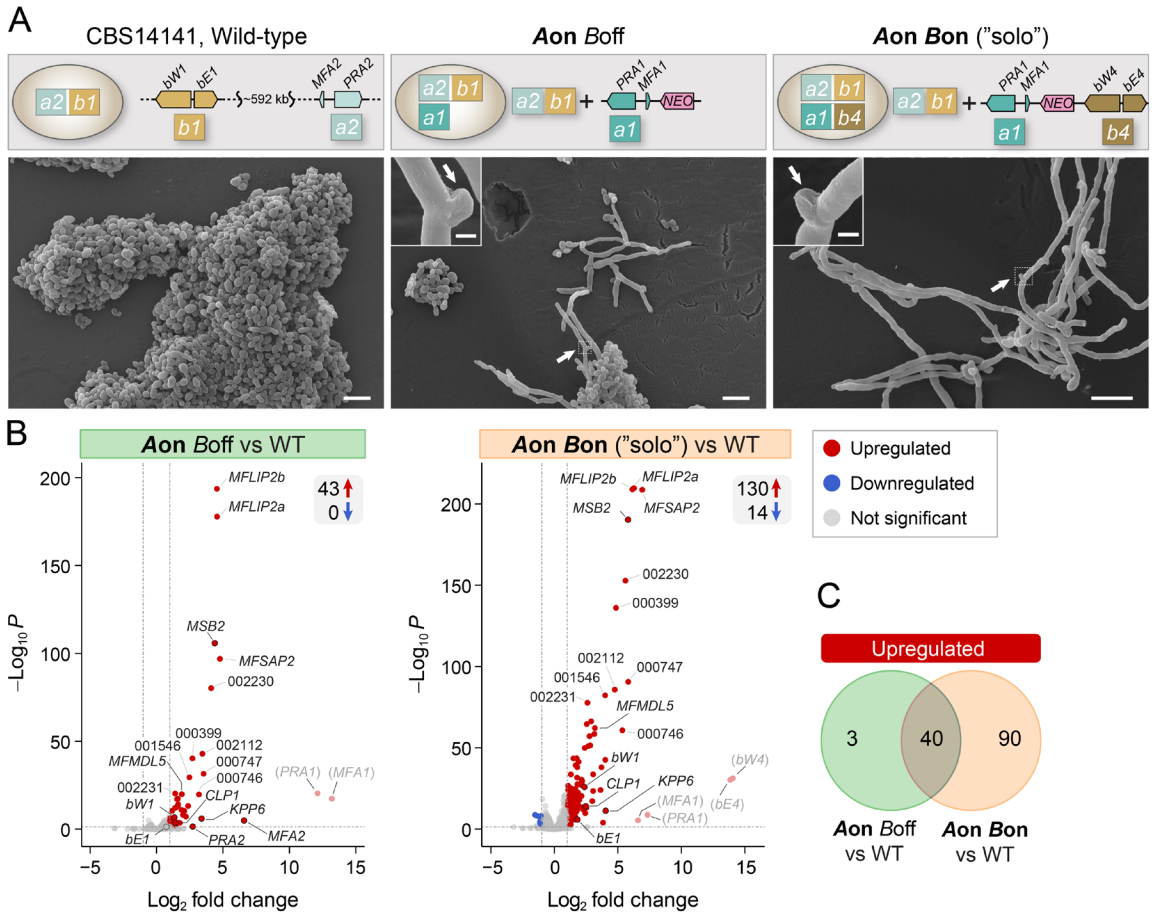

Fig. 5. *Malassezia furfur* strains expressing compatible *P/R* and *HD* genes are self-filamentous and resemble the initial stages of sexual development of other basidiomycetes. (A) Scanning electron microscopy images of *M. furfur* transformants expressing a compatible *P/R* allele (*A*on *B*off) or a compatible *P/R* and *HD* allele (*A*on *B*on, "solo") showing hyphal development (self-filamentation) and the formation of clamp-like cells (indicated by white arrows). Scale bars = 10µm (1µm in the insets). (B) Volcano plot representations of differentially expressed genes. Red and blue points represent, respectively, transcripts with significantly increased or decreased levels in *M. furfur* transformants (*A*on *B*off, and *A*on *B*on) relative to the WT, for Log_2 fold change (FC) ≥ ±1, and a false discovery rate (FDR) < 0.05. Grey dots represent transcripts with no significant changes. Faded red dots representing the expression levels of *PRA1*, *MFA1*, *bW4* and *bE4* are depicted only as internal controls as their upregulation is expected given their absence in the parental strain (i.e., only harbors the allele pairs *PRA2*/*MFA2* and *bW1*/*bE1*). (C) Venn diagram showing common and unique sets of up-regulated genes between the comparisons reported in panel B.